NUMERICAL SIMULATIONS OF CONDITIONALLY UNSTABLE FLOWS OVER A RIDGE

Mario M. Miglietta[1] and Richard Rotunno[1]

[1] ISAC-CNR, Lecce, Italy
[2] NCAR, Boulder, USA
E-mail : m.miglietta@isac.cnr.it

Abstract: Numerical simulations of conditionally unstable flows impinging on a mesoscale mountain ridge have been performed with an explicitly resolving cloud model in order to investigate the generation and the propagation of convective cells. The environmental conditions are the same studied by Chu and Lin (2000), but the horizontal resolution has been increased (grid interval = 250 *m*) in order to resolve properly the cellular-scale features. The solutions have been analyzed for different uniform-wind profiles impinging on a bell-shaped ridge 2000 *m* high.
In the experiments with weaker environmental wind speeds (U = 2.5 *m/s*, 10 *m/s*), a density current is generated during the first few hours of the experiment as a consequence of the evaporative cooling associated with the rainfall on the upstream side of the mountain. The outflow produces convective cells near the head of the current, so that no rainfall is produced close to the mountain at later times. For larger wind speeds (U = 20 *m/s*, 30 *m/s*), the orographically induced condensation is stronger and therefore the rainfall-evaporation mechanism less efficient. As a consequence, no density current is generated and the cells remain close to the mountain. Experiments with different mountain heights h show that the qualitative response of the system remains the same if the wind speed is kept constant, showing that the Froude number ($= U/N_m h$, N_m^2 moist static stability) is not a very relevant parameter in the convective case.

Keywords: *convection, orographic precipitation, mountain flows*

1. INTRODUCTION

Numerical idealized studies of deep convection in mountainous regions are relatively few and challenging since the number of control parameters is great (for example, upstream wind and temperature profiles, shape of the mountain, etc.). Chu and Lin (2000) performed numerical simulations with an horizontal resolution of 2.5 *km* and were able to identify three distinct flow regimes as a function of the Froude number (defined as $F = U/Nh$, where U is the basic state wind speed, N the Brunt-Väisälä frequency and h the mountain height). In regime I (small F), a density current and a convective system propagate upstream of the mountain; in regime II (intermediate F), the propagation speed of the density current is approximately balanced by the basic-state wind and the stationary density current and convective system remain close to the mountain; in regime III (large F), the density current is swept downstream by the relatively strong wind, leading to large precipitation accumulations on the peak or upslope. New results have been discussed in Chen and Lin (2005), where a 2D moist flow diagram regime, based on F and the Convective Available Potential Energy (*CAPE)* of the upstream sounding, has been proposed; also, a fourth regime, characterized by an orographic stratiform precipitation system over the mountain and possibly a downstream-propagating cloud system was identified.

In recent years, modern computer systems have provided the technical capacity for developing fine-grid models with resolutions as high as few hundreds of meters. At high resolution, convection can be explicitly resolved, meaning that clouds and precipitation are entirely represented through prognostic equations; thus, a better understanding of convective processes and a more reliable estimate of the associated precipitation can be gained with high-resolution numerical experiments.

In the present study, our main objective is to ascertain the dynamics of moist conditionally unstable air passing over a two-dimensional hill, revisiting the low-resolution experiments in Chu and Lin (2000) at higher resolution. Although convective dynamics is fully 3D, we analyze here the state space in the simple 2D context in order to understand the basic properties of the flow.

2. NUMERICAL SETUP

In the present study, numerical simulations have been carried out using the cloud-resolving model, with non-hydrostatic and fully nonlinear governing equations, described in Bryan and Fritsch (2002). Subgrid-

scale turbulence is parameterized using a turbulent-kinetic-energy closure; microphysical processes are parameterized through a modified version of the Lin et al. (1983) scheme, including ice; graupel is defined as a large-ice category (no hail is included). Rotational effects are neglected in the present experiments.

The domain is 320 *km* wide (in the *x* direction) and 20 *km* deep (in the *z* direction), the grid resolution *dx* = 250 *m* (apart from a few preliminary experiments, see Section 3) and the vertical spacing variable: in particular, *dz* is constant (250 *m*) at levels lower than 9000 *m*, increases to 500 *m* from 9000 *m* to 10500 *m*, remaining constant (at 500 *m*) up to the top of the domain. The horizontal extension of the domain has been chosen in order to minimize the potential spurious effects of gravity wave reflection at the inflow and outflow boundaries, where an open-radiative condition (Durran and Klemp, 1983) is applied. Also, the total outward mass flux is not allowed to exceed the total inward mass flux; this constraint helps to prevent runaway outward flux that can cause domain-total mass loss and pressure fall. The lower boundary is free-slip, while a Rayleigh damping layer is applied to the uppermost 6 *km*, serving to absorb vertically propagating waves.

The simulations are initialized using the Weisman and Klemp (1982) sounding (see also Chu and Lin (2000), Fig. 3), but with a vertically uniform atmospheric wind speed (*U*). In order to explore the state space, the value of *U* was varied for the different experiments. For simplicity, the orography was prescribed by a bell-shaped mountain:

$$h = \frac{h_m}{1+(x/a)^2} \tag{1}$$

with the half-width *a* equal to 30 *km* and the maximum height h_m equal to 2000 *m*.

3. RESULTS

Preliminary experiments, performed with the same horizontal resolution of 2.5 *km* used in Chu and Lin (2000), are able to reproduce the flow features shown in that paper. However, moving to finer and finer horizontal resolutions (500 *m*, 250 *m*), both quantitative and qualitative differences emerge. Such discrepancies can be explained taking into account that a grid spacing of less than 500 *m* is needed to resolve properly the convective cellular scale features. Therefore, a resolution of 250 *m* is used hereafter.

Figure 1 shows the time evolution of the rain water (q_r) as a function of distance across the mountain at the constant height 2 *km*, for the four experiments with different values of the atmospheric wind speed, which are 2.5 *m/s* (a), 10 *m/s* (b), 20 *m/s* (c) and 30 *m/s* (d). On the downstream side ($x>0$), the advection of convective cells associated with the lee-side hydraulic jump is a transient feature common to all the simulations, while convective cells remain statistically quasi-stationary immediately downstream of the mountain for the two largest values of *U*.

Now we pass to consider the upstream features. For the weaker wind speed of Fig. 1a, q_r is shown over a shorter time interval (5 *h*), since the fast propagation of the upstream rain cells reach the inflow boundary after only 6 *h* (and then are reflected toward the mountain). When we consider *U* = 10 *m/s* (Fig. 1b), the intensity of the cells in the proximity of the mountain weakens and the q_r-isolines move upstream only after approximately 10 *h* (fig. 1b). For the larger wind speeds of *U* = 20 *m/s* (Fig. 1c) and *U* = 30 *m/s* (Fig. 1d), the q_r-isolines remain close to the mountain during the entire simulations.

In order to understand the different behavior on the upstream side among the simulations, potential temperature perturbations are shown in Fig. 2 along vertical cross sections extending from the ground up to 5 *km*. The results are shown after about 5 *h* for *U* = 2.5 *m/s* and at the final integration time *t* = 15 *h* for the other experiments.

For *U* = 2.5 *m/s* (Fig. 2a) a density current with a minimum temperature perturbation of -8 °*C* moves quickly towards the entrance of the channel. The analysis of the first few hours (not shown) suggests that the solution does not include any upstream blocking, thus, the origin of the density current must be attributed entirely to the moist dynamics. The density current is generated as a consequence of the cooling associated with the evaporation of the rainfall in the first few hours of the simulation on the upstream side of the mountain. The outflow produces new convective cells on the upstream side of the head of the density current while no further rainfall is produced close to the mountain.

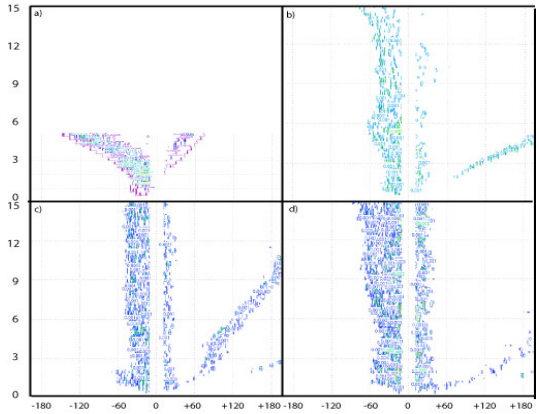

Figure 1: Time evolution of the rain water q_r in the cross-ridge direction at the constant height of 2 *km*, for four different values of atmospheric wind speed: 2.5 *m/s* (a, left top), 10 *m/s* (b, right top), 20 *m/s* (c, left bottom) and 30 *m/s* (d, right bottom). The time interval is 15 *h* (5 *h* for panel a), the contour interval 0.001 *g/kg* (0.0005 *g/kg* for panel a).

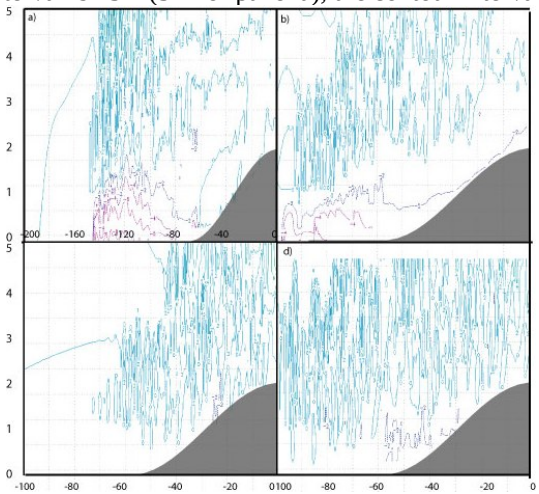

Figure 2: Potential temperature perturbations (c.i. = 2 °*C*) along vertical cross sections extending from the ground up to 5 *km*, for the different experiments: *U* = 2.5 *m/s* (a, left top), *U* = 10 *m/s* (b, right top), *U* = 20 *m/s* (c, left bottom) and *U* = 30 *m/s* (d, right bottom).The results are shown after 5 *h* for *U* = 2.5 *m/s* and at the final integration time *t* = 15 *h* for the other experiments. The domain shown is 100 *km* (200 *km* in panel a) wide on the upstream side, with the mountain top on the right border.

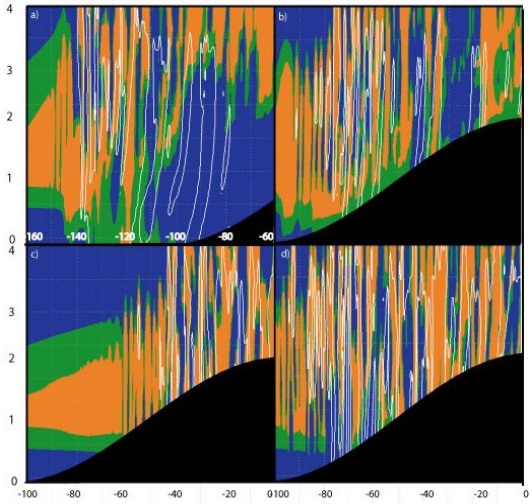

Figure 3: Relative humidity (*rh*) (blue: *rh* < 90%, green: 90% < *rh* < 98%, orange: *rh* > 98%) in a vertical cross section, extending from the ground up to 4 *km*, located upstream of the mountain for different wind speeds: *U* = 2.5 *m/s* (a, left top), *U* = 10 *m/s* (b, right top), *U* = 20 *m/s* (c, left bottom) and *U* = 30 *m/s* (d, right bottom).The results are shown after 5 *h* for *U* = 2.5 *m/s* and at the final integration time *t* = 15 *h* for the other experiments. The domain shown is 100 *km* wide (from -160 *km* to -60 *km* in panel a, from -100 *km* to the mountain top for the other cases). The white contours represent the region with rain water content larger than 0.0005 *g/kg*. The mountain is in black.

When we consider higher wind speeds (U = 10 *m/s* ; Fig. 2b), the time required for the density current to form and progressively extend upstream is larger. It takes several hours before the evaporational cooling is effective enough to generate a cold pool that starts propagating upstream. After 15 *h*, the head of the current is about 100 *km* far from the mountain (Fig. 2b), and no cells are formed any longer close to the mountain ridge (see also Fig. 1b). With further increases of wind speed (Figs. 2c-2d), the cold pool essentially disappears, and as a consequence, after a transitional phase due to the initial adjustment (Figs. 1c-1d again), the cells remains quasi-stationary on the upstream side of the mountain.

The intensity of the cooling generating the density current is dependent on the degree of saturation of the surrounding atmosphere. Considering that the condensation depends on the environmental wind speed [Rotunno and Ferretti (2001), Eq. 4.2], the larger the wind speed, the stronger the condensation and the less efficient the evaporation mechanism. Figure 3 shows the relative humidity in a vertical cross section upstream of the mountain for different wind speeds: the saturated (or quasi-saturated) regions are wider when the environmental flow is larger. For U = 2.5 *m/s* (Fig. 3a), the air is far from saturation in most of the channel, so that the rainfall, passing through unsaturated air, may evaporate, the cooling is very efficient and a density current can propagate to the upstream side of the channel. For U = 10 *m/s*, the air over the forward slope of the mountain is still mostly unsaturated (Fig. 3b) and the cooling is strong enough to generate a density current (Fig. 2b). Moving to the cases U = 20 *m/s* (Fig. 3c) and U = 30 *m/s* (Fig. 3d), the atmosphere remains mostly saturated close to the ground, the evaporation cooling is weaker and it is not able to develop a density current.

4. CONCLUSIONS

The cold air outflow, caused by the evaporative cooling of rain, is an important mechanism for the cell development and movement for small values of U. Since the air beneath a thunderstorm may be subsaturated, rain may evaporate and cool the sub-cloud layer. A density current is then generated, that spreads under its own weight, displaces air upward in its path, and may initiate new cells upstream. For large values of U, the subsaturation is confined to smaller regions and the evaporation is less effective, so that the cells remain localized close to the mountain. This interpretation is consistent with Stein (2004)'s experiments, where idealised simulations, performed with the atmospheric conditions taken from Cagliari sounding during MAP-IOP2B (Mesoscale Alpine Program-Intensive Observation Period) but with different wind speeds, showed results similar to the present study.

Mountain waves do not play any role in the present analysis; further experiments, maintaining the same F but changing U, show that the results depend mainly on U. Thus, F does not turn out to be a relevant parameter (cf. Chu and Lin 2000).

The present study is limited to 2D simulations. We are currently running their 3D counterparts to make sure that none of the features observed in the 2D experiments is an artifact of the 2D assumption. The more complex and realistic 3D experiments will be discussed in a future work.

REFERENCES

Bryan, G. H., and J. M. Fritsch, 2002: A benchmark simulation for moist nonhydrostatic models. *Mon. Wea. Rev.* **130**, 2917-2928.

Chu, C.-M., and Y.-L. Lin, 2000: Effects of orography on the generation and propagation of mesoscale convective systems in a two-dimensional conditionally unstable flow. *J.Atmos. Sci.* **57**, 3817-3837.

Chen, S.-H., and Y.-L. Lin, 2005: Effects of Moist Froude Number and CAPE on a Conditionally Unstable Flow over a Mesoscale Mountain Ridge. *J.Atmos. Sci.* **62**, 331-350.

Durran, D. R., and J. B. Klemp, 1983: A compressible model for the simulation of moist mountain waves. *Mon. Wea. Rev.* **111,** 2341–2361.

Lin, Y.-L., R. D. Farley, and H. D. Orville, 1983: Bulk parameterization of the snow field in a cloud model. *J. Appl. Meteor.* **22**, 1065–1092.

Rotunno, R., and R. Ferretti, 2001: Mechanisms of intense Alpine rainfall. *J. Atmos. Sci.* **58,** 1732–1749.

Stein, J., 2004: Exploration of some convective regimes over the Alpine orography. *Q. J. R. Meteorol. Soc.* **130**, 481–502.

Weisman, M. L., and J. B. Klemp, 1982: The dependence of numerically simulated convective storms on vertical wind shear and buoyancy. *Mon. Wea. Rev.* **119**, 504-52**.**